

## COMMUNICATION

# Structural Basis for Catalysis by the Mono- and Dimetalated Forms of the *dapE*-Encoded *N*-succinyl-L,L-Diaminopimelic Acid Desuccinylase

Boguslaw P. Nocek<sup>1</sup>†, Danuta M. Gillner<sup>2,3</sup>†, Yao Fan<sup>1</sup>,  
Richard C. Holz<sup>2\*</sup> and Andrzej Joachimiak<sup>1\*</sup>

<sup>1</sup>Midwest Center for Structural Genomics and Structural Biology Center, Argonne National Laboratory, 9700 South Cass Avenue, Argonne, IL 60439, USA

<sup>2</sup>Loyola University Chicago, Chicago, IL 60626, USA

<sup>3</sup>Silesian University of Technology, 44-100 Gliwice, Poland

Received 2 November 2009;  
received in revised form  
26 January 2010;  
accepted 27 January 2010  
Available online  
4 February 2010

Biosynthesis of lysine and *meso*-diaminopimelic acid in bacteria provides essential components for protein synthesis and construction of the bacterial peptidoglycan cell wall. The *dapE* operon enzymes synthesize both *meso*-diaminopimelic acid and lysine and, therefore, represent potential targets for novel antibacterials. The *dapE*-encoded *N*-succinyl-L,L-diaminopimelic acid desuccinylase functions in a late step of the pathway and converts *N*-succinyl-L,L-diaminopimelic acid to L,L-diaminopimelic acid and succinate. Deletion of the *dapE* gene is lethal to *Helicobacter pylori* and *Mycobacterium smegmatis*, indicating that DapE's are essential for cell growth and proliferation. Since there are no similar pathways in humans, inhibitors that target DapE may have selective toxicity against only bacteria. A major limitation in developing antimicrobial agents that target DapE has been the lack of structural information. Herein, we report the high-resolution X-ray crystal structures of the DapE from *Haemophilus influenzae* with one and two zinc ions bound in the active site, respectively. These two forms show different activity. Based on these newly determined structures, we propose a revised catalytic mechanism of peptide bond cleavage by DapE enzymes. These structures provide important insight into catalytic mechanism of DapE enzymes as well as a structural foundation that is critical for the rational design of DapE inhibitors.

© 2010 Elsevier Ltd. All rights reserved.

Edited by M. Guss

Keywords: X-ray crystallography; zinc; hydrolases; mechanism; antimicrobials

The *meso*-diaminopimelate (mDAP)/lysine biosynthetic pathway offers several potential antibacterial enzyme targets that have yet to be explored.<sup>1–3</sup> One of the products of this pathway, lysine, is required in protein synthesis and is also used in the peptidoglycan layer of Gram-positive bacterial cell walls. A second product of this pathway, mDAP is an essential component of the peptidoglycan cell

wall for Gram-negative bacteria, providing a link between polysaccharide strands. It has been shown that deletion of the gene encoding one of the enzymes in this pathway, the *dapE*-encoded *N*-succinyl-L,L-diaminopimelic acid (L,L-SDAP) desuccinylase (DapE; EC 3.5.1.18), is lethal in *Helicobacter pylori* and *Mycobacterium smegmatis*.<sup>4,5</sup> Notably, the *H. pylori* *dapE* deletion mutant was unable to grow in lysine-supplemented media, implying that lysine cannot be effectively imported. These results strongly suggest that the mDAP/lysine biosynthetic pathway is the *only* source for lysine and cannot be compensated by other pathways or import. Lysine is an essential amino acid that is not synthesized in humans; hence, it must be ingested as lysine or lysine-containing proteins. In contrast, most bacteria, plants, and algae can synthesize lysine and mDAP from aspartic acid.<sup>1,2,6</sup> Since there are no

\*Corresponding authors. E-mail addresses:  
rholz1@luc.edu; andrzej@anl.gov.

† B.P.N. and D.M.G. contributed equally to this work.  
Abbreviations used: mDAP, *meso*-diaminopimelate;  
L,L-SDAP, *N*-succinyl-L,L-diaminopimelic acid; CPG<sub>2</sub>,  
carboxypeptidase from *Pseudomonas* sp. strain RS-16;  
AAP, leucine aminopeptidase from *Aeromonas proteolytica*;  
PDB, Protein Data Bank.

similar biosynthetic pathways in mammals, including humans, inhibitors that target one or more of the enzymes in the mDAP/lysine pathway are hypothesized to exhibit selective toxicity against bacteria.<sup>1</sup>

Genes encoding DapE's have been identified in several pathogenic Gram-positive and Gram-negative bacteria such as *Acinetobacter baumannii* (MDRAB), *Mycobacterium tuberculosis*, *Escherichia coli* (O157:H7), *Bordetella pertussis*, *Vibrio cholerae*, *Rickettsia prowazekii*, *Pseudomonas aeruginosa*, *Yersinia pestis*, *H. pylori*, *Haemophilus influenzae*, *Staphylococcus aureus* (strain MRSA252), *Enterococcus faecium*, *Salmonella enterica*, and *Streptococcus pneumoniae*.<sup>4,5,7-10</sup> The fact that the DapE gene has been discovered in several multi-drug-resistant bacteria suggests that inhibitors of DapE enzymes may provide a new class of broad-spectrum antibiotics. Alignment of the DapE proteins listed above show a minimum of 49% sequence identity.<sup>11</sup> Significantly, all DapE proteins characterized to date are medium-sized, dimeric enzymes (41.6 kDa/subunit) that require zinc ions for their activity.<sup>6,12</sup> The amino acid residues that function as metal ligands in the structurally characterized M28 family members, the carboxypeptidase from *Pseudomonas* sp. strain RS-16 (CPG<sub>2</sub>) and the leucine aminopeptidase from *Aeromonas proteolytica* (AAP),<sup>6,13</sup> are fully conserved in all DapE sequences. Both CPG<sub>2</sub> and AAP possess a (μ-aquo)(μ-carboxylato)dizinc(II) core with one terminal carboxylate and one histidine residue at each metal site<sup>14,15</sup> and a similar active site has been proposed for DapE.<sup>6,11,12,16,17</sup> Interestingly, it has been reported that the "as purified" DapE enzyme contains only one tightly bound Zn(II) ion and exhibits ~60% of its total activity, similar to AAP.<sup>6,12</sup> Thus, both metal ions seem to be required for full enzymatic activity, but their individual catalytic roles appear to differ markedly.

A major limitation in understanding the catalytic mechanism of DapE and in developing novel inhibitors that specifically can target DapE is the lack of knowledge about their structure and an active-site architecture.<sup>6,18</sup> The only X-ray crystal structure reported for any DapE enzyme is an apo form of the DapE from *Neisseria meningitidis*.<sup>19</sup> The absence of metal ions in the structure makes it difficult to determine the spatial arrangement of the catalytically relevant residues that constitute the active site. While the current lack of structural data preclude definitive assignment of catalytically relevant residues, we have recently reported a three-dimensional homology model of the DapE from *H. influenzae*, using the crystal structure of the DapE from *N. meningitidis* as a template that exhibits ~54% identity to the DapE from *H. influenzae*.<sup>11</sup> In an effort to clearly define the structure of DapE enzymes along with the catalytically relevant residues that constitute the active site, we have solved the 2.0- and 2.3-Å resolution structures of the mono- and dinuclear zinc DapE enzymes from *H. influenzae*, respectively. Now that active forms of DapE have been crystallographically characterized, the critical components of the active site including substrate binding can be elucidated.

### Protein purification and X-ray structure of the DapE from *H. influenzae*

The recombinant DapE from *H. influenzae* was expressed and purified, as previously described, with minor modifications<sup>12</sup> from a stock culture kindly provided by Professor John Blanchard.<sup>6</sup> In order to obtain ultrapure protein suitable for crystallization, we further purified ~50 mg of DapE by loading it onto a Mono-Q column (5/50GL, GE Healthcare, Amersham Biosciences Corp., Piscataway, NJ, USA) that was pre-equilibrated with 10 mM Chelex-100-treated N-[2-hydroxy-1,1-bis(hydroxymethyl)ethyl]glycine buffer at pH 7.8. A flow rate of 0.5 mL min<sup>-1</sup> was used with a linear gradient of NaCl (0–0.25 M). Ultrapure DapE eluted as the first peak at ~0.15 M NaCl. The pure fractions were concentrated using a Centricon Plus 20 (Millipore Corp., Billerica, MA, USA). Purified DapE from *H. influenzae* exhibited a single band on SDS-PAGE, indicating an  $M_r=41,500$ . Protein concentrations were determined from the absorbance at 280 nm using a molar absorptivity ( $\epsilon_{280}=36,040 \text{ M}^{-1} \text{ cm}^{-1}$ ), calculated using the method developed by Gill and von Hippel.<sup>20</sup> The protein concentration determined using this molar absorptivity was in good agreement to that obtained using a Bradford assay. The concentration of DapE samples used for crystallization was ~15 mg mL<sup>-1</sup>. Individual aliquots of purified DapE were stored in liquid nitrogen until needed.

DapE's catalyze the hydrolysis of L,L-SDAP, forming L,L-diaminopimelic acid and succinate.<sup>6,12</sup> Initial rates were fit directly to the Michaelis-Menten equation to obtain the catalytic constants  $K_m$  and  $k_{cat}$ . The  $k_{cat}$  and  $K_m$  values for DapE were determined in triplicate by monitoring amide bond cleavage of L,L-SDAP<sup>10,12,21</sup> at 225 nm in Chelex-100-treated 50 mM potassium phosphate buffer, pH 7.5, and found to be  $140 \pm 10 \text{ s}^{-1}$  and  $730 \pm 15 \text{ mM}$ , respectively.<sup>12</sup>

Crystals of the dizinc form of DapE (ZnZn\_DapE) were grown at 16 °C by vapor diffusion in hanging drops containing 1 mL of precipitant solution (1 M ammonium sulfate, 0.2 M NaCl, and 0.1 M Na acetate, pH 4.4) and 1 μL of 13 mg mL<sup>-1</sup> of DapE with three equivalents of zinc. The crystals grew within 2 weeks and reached a size of 0.1 mm × 0.1 mm × 0.05 mm. These crystals belonged to the primitive orthorhombic space group  $P2_12_12_1$  with unit cell parameters  $a=44.7 \text{ \AA}$ ,  $b=95.7 \text{ \AA}$ , and  $c=185.4 \text{ \AA}$ . The asymmetric unit contains two molecules with a  $V_m$  value of 2.4 Å (solvent content, 48%). In order to determine the structure of a monometalated form of DapE, we used a second batch of protein equilibrated with only one equivalent of zinc, and crystals were grown under the same conditions as described above. Crystals of the monozinc form of DapE (Zn\_DapE) also grew within 10 days and reached a similar size with an identical morphology as crystals of ZnZn\_DapE (space group  $P2_12_12_1$  with unit cell parameters  $a=45.2 \text{ \AA}$ ,  $b=95.7 \text{ \AA}$ , and  $c=181.2 \text{ \AA}$ ).

Prior to data collection, an X-ray fluorescence spectrum was recorded for both Zn\_DapE and ZnZn\_DapE, which identified the presence of Zn ions in the protein crystals. Data collection was carried out on the 19-ID beamline of the Structural Biology Center at the Advanced Photon Source according to the procedure described previously.<sup>22</sup> Data to 2.0 and 2.3 Å were collected for Zn\_DapE and ZnZn\_DapE, respectively, at a wavelength of 0.9794 Å from the single crystals and were processed using HKL2000 (Table 1).<sup>23</sup>

The structure of Zn\_DapE was determined by molecular replacement using the crystal structure of the DapE from *N. meningitidis* as a template [Protein Data Bank (PDB) ID: 1vgy], which exhibits ~54% identity with the DapE from *H. influenzae*, as described previously.<sup>11</sup> Molecular replacement searches were completed with MOLREP (*R*-factor of 0.46%, correlation coefficient of

0.50) using the CCP4 suite.<sup>24,25</sup> Several rounds of rebuilding and readjusting using Coot and ARP/wARP were required to improve the initial model.<sup>26,27</sup> The final model was refined against all reflections using the program REFMAC 5.5<sup>28</sup> in the resolution range 30 to 2.0 Å except for 5% of the reflections, which were randomly selected and used to monitor *R*<sub>free</sub>. The final refinement statistics are presented in Table 1.

The structure of ZnZn\_DapE was determined by molecular replacement with MOLREP (*R*-factor of 0.43%, correlation coefficient of 0.52) using the catalytic domain of Zn\_DapE in the first round and then the dimerization domain of Zn\_DapE. Several cycles of model building and water picking with Coot followed by refinement with REFMAC 5.5 were undertaken to build a final structural model (Table 1). Analysis and validation of the structures were performed with the aid of MolProbity, Coot validation tools, and SSM and DALI servers.<sup>29–31</sup> Figures were prepared using the program PyMOL.<sup>32</sup>

The crystal structures of Zn\_DapE and ZnZn\_DapE from *H. influenzae* were determined at 2.0 and 2.3 Å resolution, respectively. The final model for both enzymes includes two monomers in the asymmetric unit forming a dimer. The model of Zn\_DapE contains 735 residues out of a possible 752 residues, 414 water molecules, 2 zinc ions, and 2 sulfate ions. The model of ZnZn\_DapE contains 749 residues out of 752 residues, 4 zinc ions, 212 water molecules, 2 glycerol molecules, and 5 sulfate ions. The electron density maps obtained for both structures were of high quality and allowed reliable modeling of both monomers, except in the loop regions (residues 192–198 in chain A and 193–196 and 241–245 in chain B), which are disordered and were not included in the final model. The final models exhibited good crystallographic and geometric statistics and were refined against 2.0 Å data for Zn\_DapE with a final *R*<sub>work</sub> of 20.2 and an *R*<sub>free</sub> of 25.4 and against 2.3 Å data for ZnZn\_DapE to an *R*<sub>work</sub>/*R*<sub>free</sub> of 19.4/25.0 (Table 1).

The DapE enzyme from *H. influenzae* is organized as a dimer and closely resembles the structure of the DapE from *N. meningitidis*. The search for structural homologues of DapE using the DALI and SSM programs<sup>30,31</sup> identified several closely related homologues with the apo form of DapE from *N. meningitidis* (PDB ID: 1vgy, *Z*-score = 47.8,<sup>30</sup> rmsd = 2.0<sup>31</sup>),<sup>19</sup> acetylornithine deacetylase from *Bacteroides thetaiotaomicron* VPI-5482 (PDB ID: 3ct9, *Z*-score = 32.8,<sup>30</sup> rmsd = 2.7<sup>31</sup>),<sup>33</sup> and the CPG<sub>2</sub> from *Pseudomonas* sp. strain RS-16 (PDB ID: 1cg2, *Z*-score = 31.6,<sup>30</sup> rmsd = 3.0<sup>31</sup>)<sup>34</sup> being the top three hits. Each subunit of the dimer consists of two functional domains: a large catalytic domain, which supplies the ligands for the zinc ions in the active site, and a smaller dimerization domain that contributes to dimer formation (Fig. 1). The domains are connected by a small hinge region (residues 176–179 and 298–293) allowing movement of the dimerization domain with respect to the catalytic domain. The shape of the DapE dimer resembles a rotary style phone receiver with the larger catalytic domain being

**Table 1.** Data and refinement statistics

	Zn_DapE	ZnZn_DapE
<i>Data collection statistics</i>		
Space group	P2 <sub>1</sub> 2 <sub>1</sub> 2 <sub>1</sub>	P2 <sub>1</sub> 2 <sub>1</sub> 2 <sub>1</sub>
Unit cell parameters: <i>a</i> , <i>b</i> , <i>c</i> (Å)	45.2, 95.7, 181.2	44.7, 95.7, 185.4
Wavelength (Å)	0.9794	0.9794
Resolution (Å)	30–2.03	35–2.30
Number of observed reflections	232,530	165,276
Number of unique reflections	51,964	34,773
<i>R</i> <sub>merge</sub> <sup>a</sup> (%)	7.7 (69.2)	8.6 (56.7)
Completeness (%)	99.9 (99.9)	95.9 (99.7)
1/σ	20.2 (2.5)	17.8(3.4)
<i>Phasing</i>		
Phasing method	MR	MR
Resolution range (Å)	30–3.0	35–3.0
Molecular replacement statistics CC 0.5 <i>R</i> <sub>fac</sub> 0.46		
Correlation coefficient	0.5	0.42
<i>R</i> -factor	0.46	0.52
<i>Refinement statistics</i>		
Resolution range (Å)	40.0–2.03	40.0–2.30
<i>R</i> <sub>cryst</sub> (%)	20.2	19.4
<i>R</i> <sub>free</sub> (%)	25.4	25.0
Number of non-hydrogen atoms	5718	5718
Zn ions/SO <sub>4</sub>	2/2	4/5
Solvent	401	212
<i>rmsd from target values</i>		
Bond lengths (Å)	0.017	0.015
Bond angles (°)	1.57	1.43
<i>Average B-factors (Å<sup>2</sup>)</i>		
Protein main chain	31.2	39.3
Protein side chains and solvent	35.1	41.5
Zn1/Zn2	31.7/—	34.3/35.7
Average metal occupancy	1.0/—	1.0/0.45
<i>Ramachandran Plot<sup>b</sup> (%)</i>		
Favored	97.3	97.5
Allowed	100	100
Outliers	0	0
PDB ID	3ISZ	3IC1

The values in parentheses are for the highest-resolution shell.

<sup>a</sup>  $R_{\text{merge}} = \sum_i \sum_j |I_{h,i} - \langle I_h \rangle| / \sum_i \sum_j I_{h,i}$

<sup>b</sup> As defined by MolProbity.

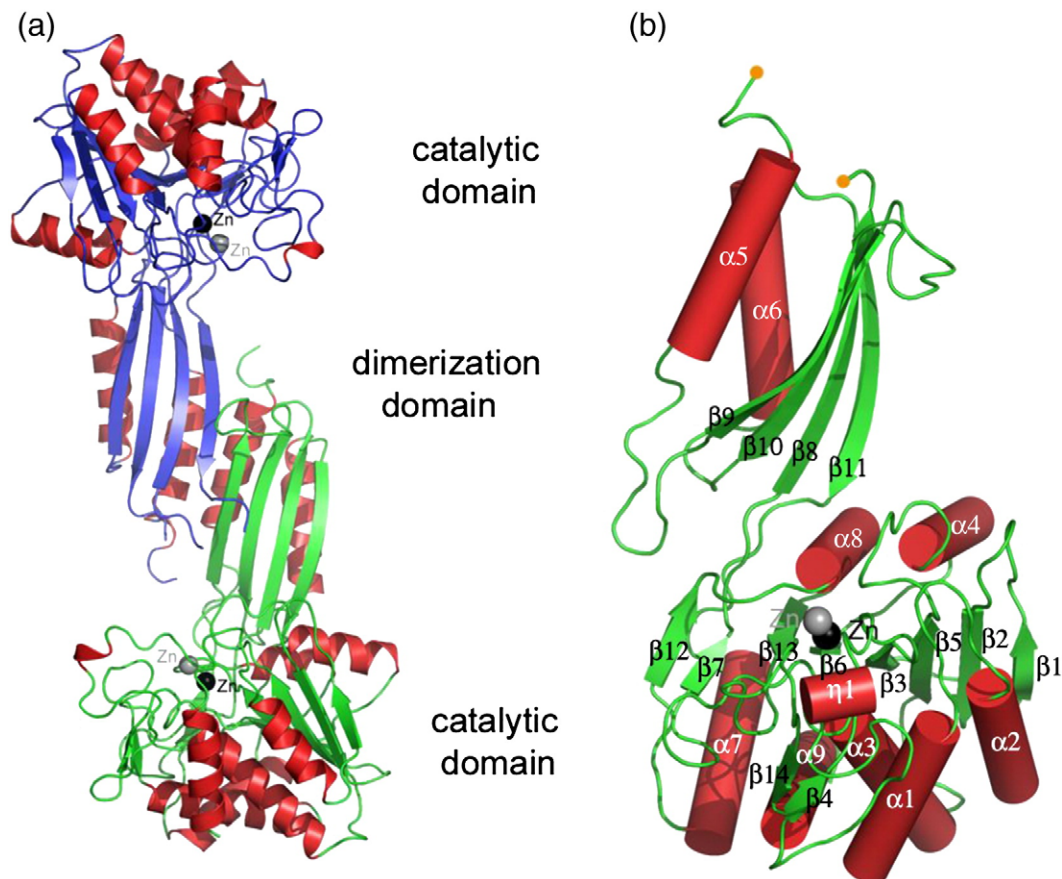


**Fig. 1.** Structure of DapE from *H. influenzae*. (a) Ribbon diagram showing the overall structure of the DapE dimer, with monomers shown in different colors (red and blue, and red and green). Individual domains are labeled and the secondary-structure elements are colored (blue and green,  $\beta$ -strand; red,  $\alpha$ -helices). (b) Diagram of the DapE monomer. The  $\alpha$ -helices are represented as cylinders, zinc ions are labeled in black (Zn1, the catalytic zinc) and gray (Zn2), and orange dots indicate a disordered loop that has not been modeled.

placed on the periphery of the dimer and separated by  $\sim 47$  Å. The subunit topology is illustrated in Fig. 1a.

The dimerization domain of DapE consists of a 114-residue insertion between strand  $\beta 7$  and helix  $\alpha 7$  of the catalytic domain (Fig. 1) and comprises residues 180–292. The insertion folds into a two-layer  $\alpha + \beta$  sandwich fold ( $\beta 8$ ,  $\alpha 5$ ,  $\beta 9$ ,  $\beta 10$ , and  $\alpha 6$ ). One layer is formed by the four  $\beta$ -strands arranged into an antiparallel  $\beta$ -sheet with an  $\sim 45^\circ$  twist across its length, while two helices sit on one site of the molecule forming a second layer. The secondary elements are organized into two  $\beta\alpha\beta$  motifs revealing a ferredoxin-like fold.

#### Active site of the DapE from *H. influenzae*

The catalytic domain is composed of residues 1–179 and 293–376. The core of the catalytic domain consists of an eight-stranded twisted  $\beta$ -sheet that is sandwiched between seven  $\alpha$ -helices. The mixed  $\beta$ -sheet is formed by two small antiparallel  $\beta$ -strands ( $\beta 1$  and  $\beta 2$ ) followed by four centrally located parallel strands ( $\beta 5$ ,  $\beta 3$ ,  $\beta 6$ , and  $\beta 13$ ) as well as smaller parallel strands ( $\beta 7$  and  $\beta 12$ ). The last two strands are rotated  $180^\circ$  and are facing in an opposite

direction from the centrally located strands. The connecting helices are located below ( $\alpha 1$ ,  $\alpha 2$ ,  $\alpha 3$ ,  $\alpha 9$ , and  $\alpha 7$ ) and above ( $\alpha 4$  and  $\alpha 8$ ) the plane of the  $\beta$ -sheet. In addition to the central sheet ( $\beta 1$ ,  $\beta 2$ ,  $\beta 5$ ,  $\beta 3$ ,  $\beta 6$ ,  $\beta 13$ ,  $\beta 7$ , and  $\beta 12$ ), there is also a second small  $\beta$ -sheet located on the surface of the molecule. This  $\beta$ -sheet consists of two shorter antiparallel  $\beta$ -strands ( $\beta 4$  and  $\beta 14$ ) (Fig. 1b). The zinc ion or ions are located near the C-terminal end of the catalytic domains at the surface of the protein (Fig. 1a and b).

The active-site cleft is located in the center of the catalytic domain above the centrally located parallel strands of the  $\beta$ -sheet ( $\beta 3$ ,  $\beta 6$ , and  $\beta 13$ ) and is covered by the loops. The location and the architecture of the active site in ZnZn\_DapE are strikingly similar to the dinuclear active sites of CPG<sub>2</sub> and AAP (Fig. 2).<sup>34,35</sup> The two zinc ions in ZnZn\_DapE are 3.36 Å apart compared with 3.45 Å for AAP and 3.25 Å for CPG<sub>2</sub>.<sup>15,36</sup> Like AAP and CPG<sub>2</sub>, each of the zinc ions in ZnZn\_DapE adopts a distorted tetrahedral or TBP geometry with the N<sup>c</sup> nitrogen of His67 for Zn1 and H349 for Zn2 along with a bridging water/hydroxide oxygen atom making up the axial positions of a potential TBP geometry. Identical with CPG<sub>2</sub> and AAP, each zinc ion is coordinated by one imidazole group (H67 for Zn1

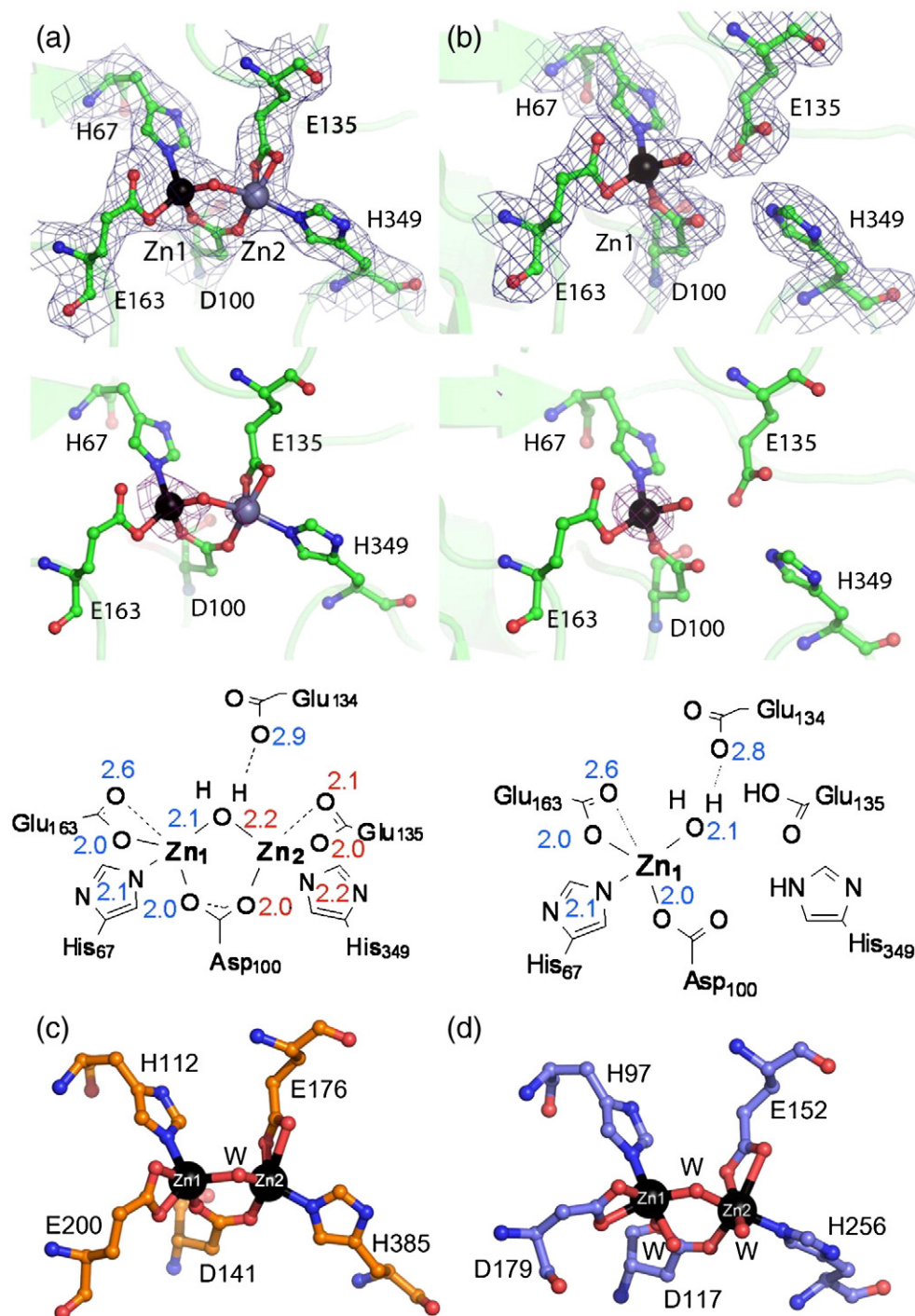


**Fig. 2.** Close-up view showing the active site of ZnZn\_DapE (a) and Zn\_DapE (b) with  $2F_o - F_c$  electron density map (blue) contoured at  $1.0\sigma$ , zinc anomalous difference Fourier maps contoured at  $4\sigma$  (magenta), and drawings of the active sites with distances displayed in angstroms. Zinc ions are labeled in black (Zn1, the catalytic zinc) and gray (Zn2). (c) Active site of carboxypeptidase G2 (PDB ID: 1cg2) and (d) close-up view of the active site of a bacterial leucyl aminopeptidase (PDB ID: 2DEA).

and H349 for Zn2) and the carboxylate oxygens of E163 (OE1 and the dangling oxygen OE2) for Zn1 and E135 for Zn2 (OE1 and the dangling oxygen OE2). Both zinc ions are bridged by D100 and a water/hydroxide. Interestingly, in the ZnZn\_DapE structure, the Zn2 binding site exhibits only ~50% occupancy. This structure confirms that the zinc ions

in DapE form a  $(\mu\text{-aquo})(\mu\text{-carboxylato})\text{dizinc(II)}$  core similar to AAP and CPG<sub>2</sub> and are consistent with EXAFS data.<sup>16</sup>

Similar to AAP, it was shown that the as-purified DapE enzyme contains only one tightly bound zinc ion and exhibits ~60% of its total activity in the presence of one zinc ion.<sup>12,37</sup> Because DapE's can be

activated with one zinc ion, it has been hypothesized that one divalent metal binding site is likely filled preferentially. This begs the following question: which metal ion binding site is filled first in the active site and which site is critical for catalysis? Therefore, we attempted to obtain structural data for a mono-zinc form of DapE (Zn\_DapE) by limiting the amount of divalent metal ions present during the crystallization process (Fig. 2). The Zn(II) ion in Zn\_DapE resides in a distorted tetrahedral or TBP geometry with the N<sup>ε</sup> nitrogen of His67 (2.1 Å) and the bridging water/hydroxide oxygen atom (2.1 Å) making up the axial positions of a potential TBP geometry. The remaining ligands are coordinated by the carboxylate oxygens of D100 (OD1, 2.0 Å) and E163 (OE, 2.0 Å, and the dangling oxygen OE2, 2.6 Å). Therefore, this structure confirms that the H67 site (Zn1) of the DapE active site is the high-affinity site and is occupied first and, hence, corresponds to the catalytic zinc. This observation is also consistent with ZnZn\_DapE structural data where we observed the same site being fully occupied and the second site being only partly occupied.

The structure of the monometalated form of DapE is only the second monometalated structure for any M28 family metalloprotease<sup>38</sup> and is reminiscent of the monometalated structures of M24 family metalloproteases, namely, the aminopeptidase P from *E. coli* and the methionine aminopeptidase from *E. coli*.<sup>39,40</sup> Given that the vast majority of proteases that can bind two metal ions are active in the presence of one metal ion, the X-ray structure of the Zn\_DapE enzyme reported herein provides a structural model for the monometalated forms of these enzymes.

The structures of Zn\_DapE and ZnZn\_DapE along with the previously reported divalent metal binding studies<sup>12</sup> provide insight into the observed metal binding properties of DapE as well as all M28 metalloproteases.<sup>12</sup> Based on our X-ray crystallographic data, metal binding to DapE occurs in a sequential fashion with the first zinc binding site (Zn1) bound to the H67 site of the active site and the second zinc ion binding to H349 (Zn2). EPR and electronic absorption data on the Co(II)-substituted forms of WT and mutant DapE enzymes also indicate very clearly that the first metal ion to bind to DapE resides in the H67 site of the active site whereas the second metal binding site corresponds to the H349 site of the active site,<sup>11,12</sup> consistent with our X-ray crystallographic data. These data are significant because substrate and also inhibitor zinc-binding groups have been hypothesized to bind to Zn1.<sup>11</sup> Also of importance is that these data highlight the potential formation of heterodimetallic sites in DapE similar to AAP.<sup>41</sup> The H67 residue in DapE corresponds to H97 in AAP while H349 corresponds to H256 in AAP. Based on the crystal structure of the butane boronic acid inhibited form of AAP,<sup>42</sup> H97 (H67 in DapE) was proposed to function as a ligand in the *second* metal binding site. This apparent reversal of the zinc ion binding

sites in DapE *versus* AAP may likely indicate that the catalytic roles of the active site zinc ions in DapE's are switched from that proposed for AAP. The latter suggestion is not necessarily surprising since AAP cleaves from the N-terminus while DapE cleaves the equivalent of a C-terminal carboxylate group.

Finally, several potentially important hydrogen-bonding interactions also exist in the active site of both Zn\_DapE and ZnZn\_DapE. Perhaps most notably, there is at least one interaction between the metal-bound water/hydroxide molecule and the carboxylate oxygen atoms of Glu134. Glu134 was recently shown to be essential for catalysis and functions as a general acid/base.<sup>17</sup> Glu134 forms a strong hydrogen bond (~2.8 Å) with the terminal metal-bound water/hydroxide in Zn\_DapE and also with the bridging water/hydroxide (~2.9 Å) in ZnZn\_DapE. Other potentially important hydrogen-bonding interactions occur between the N<sup>δ</sup> proton of His67 with a side-chain oxygen of Asp69 forming an Asp-His-Zn triad that has been postulated to decrease the Lewis acidity of zinc ions<sup>43</sup> and may further assist in facilitating the coordination of a double-bonded oxygen to Zn2. Similar arrangement and a fully conserved Asp-His-Zn triad are observed for both AAP and CPG<sub>2</sub> and are postulated to regulate the Lewis acidity of the zinc ion.<sup>36</sup>

### Inhibitor design implications for DapE enzymes

Inspection of the Zn\_DapE and ZnZn\_DapE structures, combined with surface analysis, reveals a smile-shaped cavity that extends along the catalytic domain and surrounds the active site (Fig. 3). This well-defined and negatively charged cavity is shaped from the top by strand β12 and α8 and in the middle by the loop connecting these two elements. The bottom of the cavity is formed by loops (loop connecting β-strands β6 and β7 and loop connecting β5 and α4) and α4. Taking into account the linear character of the substrate, it is likely that the substrate binds in an extended conformation along the smile-shaped groove with the peptide bond positioned over the active-site metal ions while the rest of the substrate could be further stabilized by the interaction of carboxyl groups of the substrate with the surrounding residues (Fig. 4). Assuming that the carbonyl moiety of the peptide bond binds to one or both metal ions in the active site, two residues, E134 and T325, likely form hydrogen bonds with the carbonyl group and/or the backbone amine group of L,L-SDAP. E134 had been shown to function as the general acid/base during catalysis, suggesting that T325, which is centrally positioned on the loop overhanging the active site, may play an important role in substrate recognition and transition-state stabilization. It is easy to envision this loop undergoing movements upon substrate binding.

DapE enzymes have been shown to exhibit strict specificity for the L,L-isoform of SDAP,

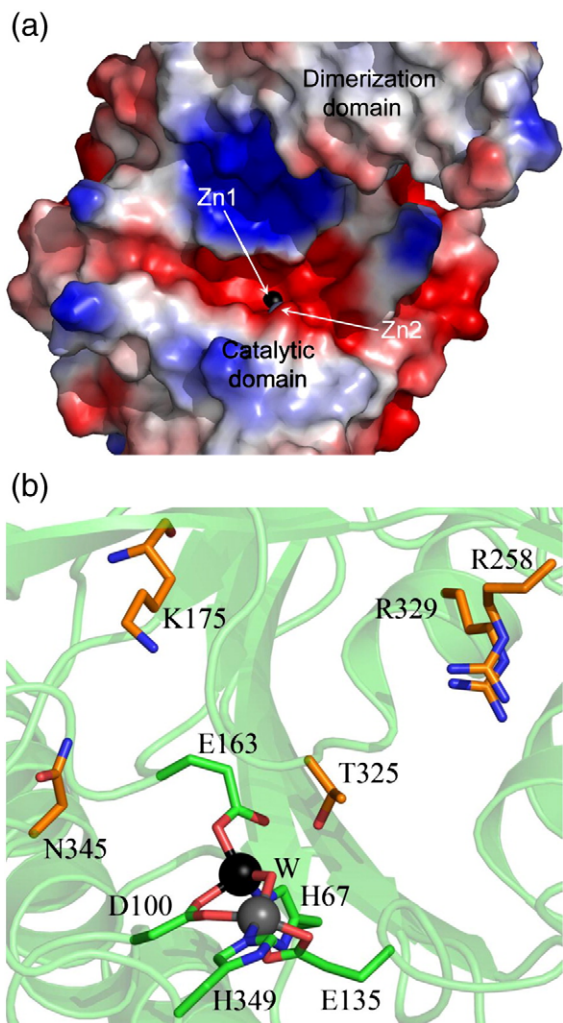


**Fig. 3.** (a) Surface rendering of the ZnZn\_DapE molecule (molecule A is shown) showing the charge distribution and depicting the smile-shaped active-site cavity. The surface charge distribution was determined using PyMOL. (b) Close-up view of the active-site cavity of ZnZn\_DapE, molecule A, showing charged residues that may interact with the substrate. The zinc ions are represented as gray and black (catalytic zinc) spheres. Side chains of residues that may be involved in recognizing and binding the substrate are shown as orange sticks. Figures were prepared using PyMOL.

indicating that the DapE active site is highly specific in both functional group recognition as well as stereochemistry.<sup>12</sup> This specificity is built into the substrate binding pocket, which will minimize the nonspecific interactions of DapE with nonproductive inhibitors.<sup>44,45</sup> Therefore, it is quite likely that substrate binding is further controlled by interactions of the substrate carboxylic groups with positively charged amino acid side chains. The potential positively charged residues that could interact with the carboxylic groups of the substrate are K175, R178, and N345 at one end and R258, R329, and K139 at the opposite end. The K175 side chain is within  $\sim 6$  Å of the center of the active site; hence, it is easy to

envision the  $\epsilon$ -amino group of the lysine side chain within the appropriate distance to form a salt bridge interaction with a substrate carboxylate group and, thus, be involved in recognizing and binding substrate. On the opposite side, carboxylate groups of *L,L*-SDAP could also be further stabilized by an interaction with R258 and/or R329. In one of the monomers of the ZnZn\_DapE structure, both of these residues form a charged dipole interaction with a sulfate ion, a possible mimic of the carboxylic group of the substrate. R329 is centrally positioned in a positively charged pocket that it forms together with R258 and is further complimented by the N-terminus of  $\alpha 8$ . These data, in combination with previously reported inhibitor binding studies,<sup>12,16,44,45</sup> indicate that DapE represents an excellent target for a highly specific drug that should have high efficacy and low toxicity.

### Mechanistic implications

The X-ray structures of Zn\_DapE and ZnZn\_DapE presented herein provide a structural foundation for the corroboration of the proposed reaction mechanism of DapE.<sup>6,12,17</sup> Analysis of structures and previously reported kinetic and spectroscopic studies on DapE enzymes allows us to propose a refined mechanism of catalysis for DapE's (Fig. 4). Based on the recently proposed mechanism for AAP,<sup>46,47</sup> the first step in catalysis for DapE's is likely recognition of the *L,L*-SDAP side chain by the smile-shaped cavity adjacent to the Zn1 site. Next, the peptide carbonyl oxygen of *L,L*-SDAP coordinates to Zn1, expanding its coordination number from four to five, activating it for nucleophilic attack. Deprotonation of the metal-bound water molecule by E134 to form a nucleophilic hydroxide moiety is consistent with the postulated  $pK_a$  of the zinc-bound water molecule.<sup>6</sup> Once the zinc-bound hydroxide is formed, it can attack the activated carbonyl carbon of the substrate, forming an  $\eta$ -1- $\mu$ -transition-state complex.<sup>16</sup> Solvent kinetic isotope effect studies yielded an inverse isotope effect that was explained by the attack of a zinc-bound hydroxide on the amide carbonyl.<sup>6</sup> E134 may provide a proton to the penultimate amino nitrogen, similar to that observed for AAP, returning it to its ionized state, thus facilitating product release. Once the products are released, a water molecule bridging the two metal ions is replaced. In the absence of a second metal ion, the catalytic mechanism does not likely change markedly as H349 is in position to assist in orienting the substrate properly in the active site through the formation of a hydrogen bond with a carboxylate side chain of the substrate, thereby stabilizing the transition-state intermediate reminiscent to proposals for the monometalated forms of AAP and the methionine aminopeptidase from *E. coli*.<sup>40,48,49</sup> In the presence of a dinuclear site, the second metal ion likely coordinates either the peptide carbonyl oxygen in a bridging fashion or a carboxylate side chain of the substrate.

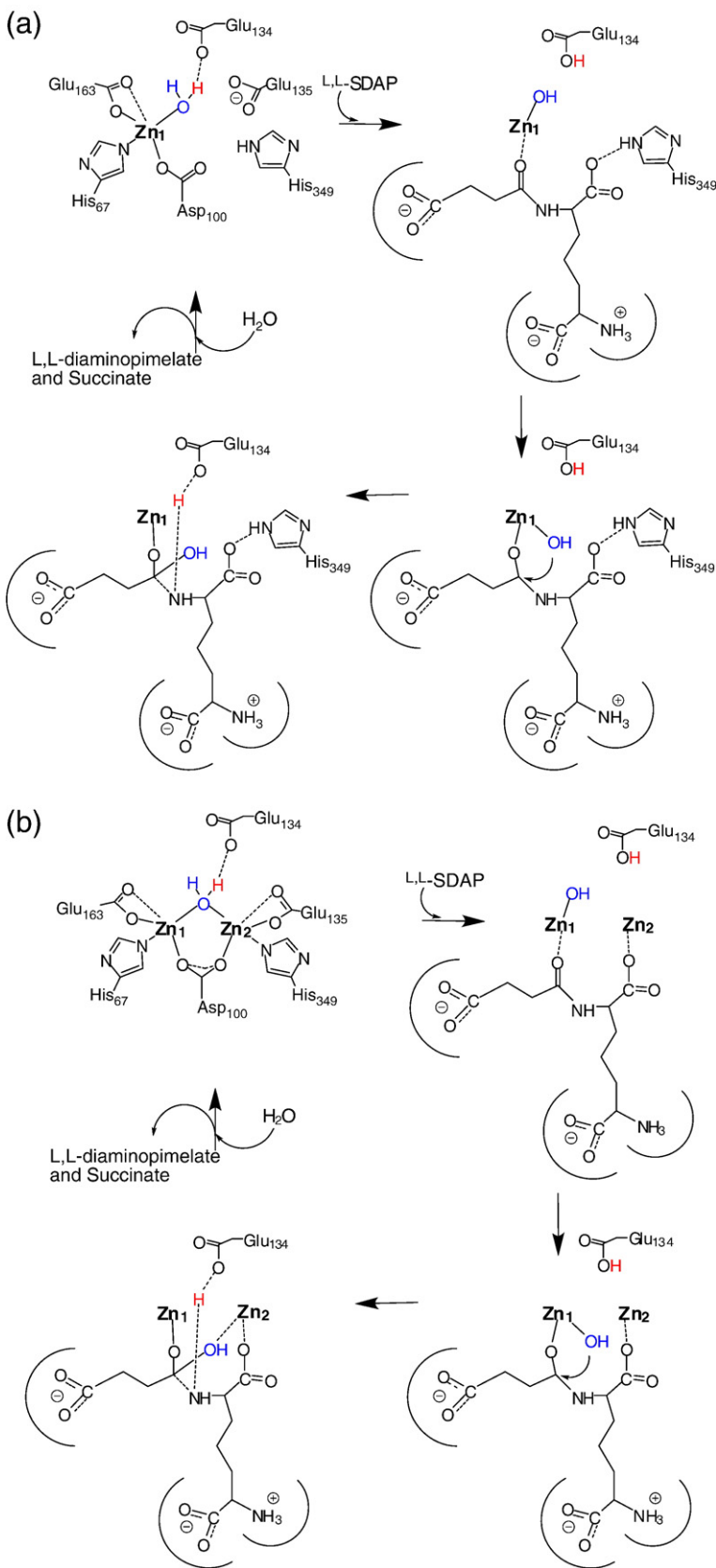


**Fig. 4.** Proposed catalytic reaction mechanisms of (a) monozinc DapE and (b) dizinc DapE.

#### PDB accession numbers

The atomic coordinates and structure factor files for the structures of Zn\_DapE and ZnZn\_DapE

from *H. influenzae* have been deposited in the Research Collaboratory for Structural Bioinformatics PDB with accession codes 3ISZ and 3IC1, respectively.

## Acknowledgements

The authors are grateful to all members of the Structural Biology Center at Argonne National Laboratory for their help in conducting these experiments. This work was supported by the National Science Foundation (CHE-0652981, R.C.H.), the National Institutes of Health (GM074942, A.J.), and the U.S. Department of Energy, Office of Biological and Environmental Research, under contract DE-AC02-06CH11357 (A.J.).

## References

- Scapin, G. & Blanchard, J. S. (1998). Enzymology of bacterial lysine biosynthesis. *Adv. Enzymol.* **72**, 279–325.
- Born, T. L. & Blanchard, J. S. (1999). Structure/function studies on enzymes in the diaminopimelate pathway of bacterial cell wall biosynthesis. *Curr. Opin. Chem. Biol.* **3**, 607–613.
- Girodeau, J.-M., Agouridas, C., Masson, M., Pineau, R. & LeGoffic, F. (1986). The lysine pathway as a target for a new genera of synthetic antibacterial antibiotics? *J. Med. Chem.* **29**, 1023–1030.
- Karita, M., Etterbeek, M. L., Forsyth, M. H., Tum-muru, M. R. & Blaser, M. J. (1997). Characterization of *Helicobacter pylori* dapE and construction of a conditionally lethal dapE mutant. *Infect. Immun.* **65**, 4158–4164.
- Pavelka, M. S. & Jacobs, W. R. (1996). Biosynthesis of diaminopimelate, the precursor of lysine and a component of peptidoglycan, is an essential function of *Mycobacterium smegmatis*. *J. Bacteriol.* **178**, 6496–6507.
- Born, T. L., Zheng, R. & Blanchard, J. S. (1998). Hydrolysis of *N*-succinyl-L,L-diaminopimelic acid by the *Haemophilus influenzae* dapE-encoded desuccinylase: metal activation, solvent isotope effects, and kinetic mechanism. *Biochemistry*, **37**, 10478–10487.
- Bouvier, J., Richaud, C., Higgins, W., Böglér, O. & Stragier, P. (1992). Cloning, characterization, and expression of the dapE gene of *Escherichia coli*. *J. Bacteriol.* **174**, 5265–5271.
- Fuchs, T. M., Schneider, B., Krumbach, K., Eggeling, L. & Gross, R. (2000). Characterization of the *Bordetella pertussis* diaminopimelate (DAP) biosynthesis locus identifies dapC, a novel gene coding for an *N*-succinyl-L,L-DAP aminotransferase. *J. Bacteriol.* **182**, 3626–3631.
- Shaw-Reid, C. A., McCormick, M. M., Sinskey, A. J. & Stephanopoulos, G. (1999). Flux through the tetrahydrodipicolinate succinylase pathway is dispensable for L-lysine production in *Corynebacterium glutamicum*. *Appl. Microbiol. Biotechnol.* **51**, 325–333.
- Lin, Y., Myhrman, R., Schrag, M. L. & Gelb, M. H. (1988). Bacterial *N*-succinyl-L-diaminopimelic acid desuccinylase. Purification, partial characterization, and substrate specificity. *J. Biol. Chem.* **263**, 1622–1627.
- Gilner, D. M., Bienvenue, D. L., Nocek, B. P., Joachimiak, A., Zachary, V., Bennett, B. & Holz, R. C. (2009). The dapE-encoded *N*-succinyl-L,L-diaminopimelic acid desuccinylase from *Haemophilus influenzae* contains two active site histidine residues. *J. Biol. Inorg. Chem.* **14**, 1–10.
- Bienvenue, D. L., Gilner, D. M., Davis, R. S., Bennett, B. & Holz, R. C. (2003). Substrate specificity, metal binding properties, and spectroscopic characteriza-tion of the dapE-encoded-*N*-succinyl-L,L-diaminopi-melic acid desuccinylase from *Haemophilus influenzae*. *Biochemistry*, **42**, 10756–10763.
- Makarova, K. S. & Grishin, N. V. (1999). The Zn-peptidase superfamily: functional convergence after evolutionary divergence. *J. Mol. Biol.* **292**, 11–17.
- Chevrier, B., Schalk, C., D'Orchymont, H., Rondeau, J.-M., Moras, D. & Tarnus, C. (1994). Crystal structure of *Aeromonas proteolytica* aminopeptidase: a prototyp-ical member of the co-catalytic zinc enzyme family. *Structure*, **2**, 283–291.
- Greenblatt, H. M., Almog, O., Maras, B., Spungin-Bialik, A., Barra, D., Blumberg, S. & Shoham, G. (1997). *Streptomyces griseus* aminopeptidase: x-ray crystallographic structure at 1.75 Å resolution. *J. Mol. Biol.* **265**, 620–636.
- Cosper, N. J., Bienvenue, D. L., Shokes, J. E., Gilner, D. M., Tsukamoto, T., Scott, R. & Holz, R. C. (2004). The dapE-encoded *N*-succinyl-L,L-diaminopimelic acid desuccinylase from *Haemophilus influenzae* is a dinuclear metallohydrolase. *J. Am. Chem. Soc.* **125**, 14654–14655.
- Davis, R., Bienvenue, D., Swierczek, S. I., Gilner, D. M., Rajagopal, L., Bennett, B. & Holz, R. C. (2006). Kinetic and spectroscopic characterization of the E134A- and E134D-altered dapE-encoded *N*-succinyl-L,L-diamino-pimelic acid desuccinylase from *Haemophilus influenzae*. *J. Biol. Inorg. Chem.* **11**, 206–216.
- Velasco, A. M., Leguina, J. I. & Lazcano, A. (2002). Molecular evolution of the lysine biosynthetic path-ways. *J. Mol. Evol.* **55**, 445–459.
- Badger, J., Sauder, J. M., Adams, J. M., Antonysamy, S., Bain, K., Bergseid, M. G. *et al.* (2005). Structural analysis of a set of proteins resulting from a bacterial genomics project. *Proteins*, **60**, 787–796.
- Gill, S. C. & von Hippel, P. H. (1989). Calculation of protein extinction coefficients from amino acid se-quence data. *Anal. Biochem.* **182**, 319–326.
- Bergmann, M. & Stein, W. H. (1939). Naphthalene-beta-sulfonic acid as a reagent for amino acids. *J. Biol. Chem.* **129**, 609–618.
- Nocek, B., Mulligan, R., Bargassa, M., Collart, F. & Joachimiak, A. (2008). Crystal structure of aminopep-tidase N from human pathogen *Neisseria meningitidis*. *Proteins*, **70**, 273–279.
- Otwinowski, Z. & Minor, W. (1997). Processing of X-ray diffraction data collected in oscillation mode. *Macromol. Crystallogr., Part A*, **276**, 307–326.
- Vagin, A. & Teplyakov, A. (2000). An approach to multi-copy search in molecular replacement. *Acta Crystallogr., Sect. D: Biol. Crystallogr.* **56**, 1622–1624.
- Collaborative Computational Project, Number 4. (1994). The CCP4 suite: programs for protein crystal-lography. *Acta Crystallogr., Sect. D: Biol. Crystallogr.* **50**, 760–763.
- Emsley, P. & Cowtan, K. (2004). Coot: model-building tools for molecular graphics. *Acta Crystallogr., Sect. D: Biol. Crystallogr.* **60**, 2126–2132.
- Morris, R. J., Perrakis, A. & Lamzin, V. S. (2003). ARP/wARP and automatic interpretation of protein elec-tron density maps. *Methods Enzymol.* **374**, 229–244.
- Murshudov, G. N., Vagin, A. A. & Dodson, E. J. (1997). Refinement of macromolecular structures by the maximum-likelihood method. *Acta Crystallogr., Sect. D: Biol. Crystallogr.* **53**, 240–255.
- Davis, I. W., Leaver-Fay, A., Chen, V. B., Block, J. N., Kapral, G. J., Wang, X. *et al.* (2007). MolProbity: all-atom contacts and structure validation for proteins and nucleic acids. *Nucleic Acids Res.* **35**, W375–383.

30. Holm, L. & Sander, C. (1998). Touring protein fold space with Dali/FSSP. *Nucleic Acids Res.* **26**, 316–319.
31. Krissinel, E. & Henrick, K. (2004). Secondary-structure matching (SSM), a new tool for fast protein structure alignment in three dimensions. *Acta Crystallogr., Sect. D: Biol. Crystallogr.* **60**, 2256–2268.
32. DeLano, W. L. (2004). *The PyMOL Molecular Graphics System*. DeLano Scientific LLC, San Carlos, CA, <http://www.pymol.org>.
33. JCSG. (2008). Crystal structure of a putative zinc peptidase (NP\_812461.1) from *Bacteroides thetaiotaomicron* VPI-5482 at 2.31 Å resolution. PDB\_code 3CT9.
34. Rowsell, S., Pauptit, R. A., Tucker, A. D., Melton, R. G., Blow, D. M. & Brick, P. (1997). Crystal structure of carboxypeptidase G2, a bacterial enzyme with applications in cancer therapy. *Structure*, **5**, 337–347.
35. Chevrier, B., D'Orchymont, H., Schalk, C., Tarnus, C. & Moras, D. (1996). The structure of the *Aeromonas proteolytica* aminopeptidase complexed with a hydroxamate inhibitor. Involvement in catalysis of Glu151 and two zinc ions of the cocatalytic unit. *Eur. J. Biochem.* **237**, 393–398.
36. Desmarais, W., Bienvenue, D. L., Bzymek, K. P., Petsko, G. A., Ringe, D. & Holz, R. C. (2006). The high-resolution structures of the neutral and the low pH crystals of aminopeptidase from *Aeromonas proteolytica*. *J. Biol. Inorg. Chem.* **11**, 398–408.
37. Prescott, J. M., Wilkes, S. H., Wagner, F. W. & Wilson, K. J. (1971). *Aeromonas* aminopeptidase improved isolation and some physical properties. *J. Biol. Chem.* **246**, 1756–1764.
38. Shi, D., Yu, X., Roth, L., Tuchman, M. & Allewell, N. M. (2007). Structure of a novel *N*-acetyl-L-citrulline deacetylase from *Xanthomonas campestris*. *Biophys. Chem.* **126**, 86–93.
39. Graham, S. C., Bond, C. S., Freeman, H. C. & Guss, J. M. (2005). Structural and functional implications of metal ion selection in aminopeptidase P, a metalloprotease with a dinuclear metal center. *Biochemistry*, **44**, 13820–13836.
40. Ye, Q. Z., Xie, S. X., Ma, Z. Q., Huang, M. & Hanzlik, R. P. (2006). Structural basis of catalysis by mono-metalated methionine aminopeptidase. *Proc. Natl Acad. Sci. USA*, **103**, 9470–9475.
41. Bennett, B. & Holz, R. C. (1997). Spectroscopically distinct cobalt(II) sites in heterodimetallic forms of the aminopeptidase from *Aeromonas proteolytica*: characterization of substrate binding. *Biochemistry*, **36**, 9837–9846.
42. DePaola, C. C., Bennett, B., Holz, R. C., Ringe, D. & Petsko, G. A. (1999). 1-Butaneboronic acid binding to *Aeromonas proteolytica* aminopeptidase: a case of arrested development. *Biochemistry*, **38**, 9048–9053.
43. Christianson, D. & Cox, D. (1999). Catalysis by metal-activated hydroxide in zinc and manganese metalloenzymes. *Annu. Rev. Biochem.* **68**, 33–57.
44. Gillner, D. M., Armoush, N., Holz, R. C. & Becker, D. (2009). Inhibitors of bacterial *N*-succinyl-L,L-diaminopimelic acid desuccinylase (DapE) and demonstration of in vitro antimicrobial activity. *Bioorg. Med. Chem. Lett.* **19**, 6350–6352.
45. Vaněk, V., Pícha, J., Buděšínský, M., Šanda, M., Jiráček, J., Holz, R. C. & Hlavacek, J. (2010). Synthesis of *N*-succinyl-L,L-diaminopimelic acid mimetics via selective protection. *Protein Pept. Lett.* **17**, 405–409.
46. Ustynyuk, L., Bennett, B., Edwards, T. & Holz, R. C. (1999). Inhibition of the aminopeptidase from *Aeromonas proteolytica* by aliphatic alcohols. Characterization of the hydrophobic substrate recognition site. *Biochemistry*, **38**, 11433–11439.
47. Stamper, C. C., Bienvenue, D. L., Bennett, B., Ringe, D., Petsko, G. A. & Holz, R. C. (2004). Spectroscopic and X-ray crystallographic characterization of bestatin bound form of the aminopeptidase from *Aeromonas proteolytica*. *Biochemistry*, **43**, 9620–9628.
48. Copik, A. J., Swierczek, S. I., Lowther, W. T., D'souza, V. M., Matthews, B. W. & Holz, R. C. (2003). Kinetic and spectroscopic characterization of the H178A mutant of the methionyl aminopeptidase from *Escherichia coli*. *Biochemistry*, **42**, 6283–6292.
49. Holz, R. C. (2002). The aminopeptidase from *Aeromonas proteolytica*: structure and mechanism of cocatalytic metal centers involved in peptide hydrolysis. *Coord. Chem. Rev.* **232**, 5–26.